

# 8

## The Passive Dendritic Tree

### OUTLINE

8.1 The Discrete Passive Tree	109	8.5 The Equivalent Cylinder*	116
8.2 Eigenvector Expansion	111	8.6 Branched Eigenfunctions*	118
8.3 Numerical Methods	113	8.7 Summary and Sources	120
8.4 The Passive Dendrite Equation	114	8.8 Exercises	121

As we observed at the outset of Chapter 6, the straight cable is an idealization. In reality, neurons exhibit an incredible variety of branching patterns. We offer six representatives in Figure 8.1 and note that though they vary greatly in both size and number of dendritic branches, each cell is a tree (no closed loops) with a well defined cell body, or soma. In this chapter we append a soma and a pair of branches to the simple passive cable of Chapter 6. We demonstrate that each of the mathematical and computational tools developed for the cable have natural extensions to the tree. We proceed to investigate synaptic integration and attenuation, with particular attention to the role played by tree eigenfunctions. We also specify and analyze the conditions under which the response of the tree may be well approximated by that of a simple straight cable.

### 8.1 THE DISCRETE PASSIVE TREE

We work in the concrete context of Figure 8.2 on the way to a more general understanding. We have indexed the compartments, following an observation of Hines, in a manner that leads to minimal fill-in in the LU factorization, Exercise 5.2, of the resulting linear system associated with the backward Euler and trapezoid schemes. The physical lengths and radii of the 3 fibers are

$$\ell_1, \ell_2, \ell_3 \quad \text{and} \quad a_1, a_2, a_3$$

respectively, while the length of each compartment, except the soma, is  $dx$ . The soma is presumed to have surface area  $A_s$  and is not typically further compartmentalized.

If we inject  $I_{stim}$  at the soma then Kirchoff's Current Law, at the node with potential  $v_{3,4}$ , requires

$$I_{stim} = C_m A_s v'_{3,4} + g_{Cl} A_s v_{3,4} + a_3^2 \pi (v_{3,4} - v_{3,3}) / (dx R_a) \tag{8.1}$$

while at the branch point ( $v_{3,1}$ ) we find

$$\frac{\pi a_3^2 (v_{3,2} - v_{3,1})}{R_a dx} = \frac{\pi a_2^2 (v_{3,1} - v_{2,4})}{R_a dx} + \frac{\pi a_1^2 (v_{3,1} - v_{1,4})}{R_a dx} + 2\pi a_3 dx (C_m v'_{3,1} + g_{Cl} v_{3,1}).$$

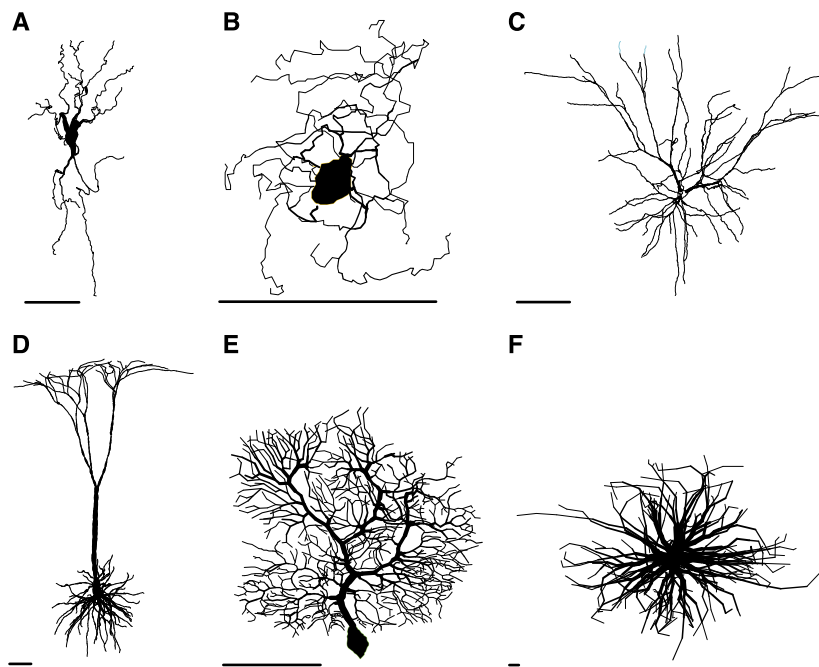


**FIGURE 8.1** Dendritic diversity. **A.** A neuron of the vagal motor pathway, part of the autonomic nervous system. **B.** A neuron of the olivary body in the brainstem. **C.** A pyramidal cell of the cortex, from layer 2/3. **D.** A pyramidal cell of the cortex, from layer 5. **E.** A Purkinje cell from the cerebellum. **F.** An  $\alpha$ -motoneuron from the spinal cord. Each scale bar is 100  $\mu\text{m}$  long. From [Segev \(1998\)](#).

Current balance at the remaining nodes proceeds exactly as before, recall Eq. (6.5). In particular, with  $\lambda_j^2 \equiv a_j/(2R_{agCl})$ , the squared space constant of branch  $j$ , we find

$$\begin{aligned}
 \tau v'_{1,1} + v_{1,1} - \lambda_1^2(v_{1,2} - v_{1,1})/dx^2 &= 0 \\
 \tau v'_{1,2} + v_{1,2} - \lambda_1^2(v_{1,3} - 2v_{1,2} + v_{1,1})/dx^2 &= 0 \\
 \tau v'_{1,3} + v_{1,3} - \lambda_1^2(v_{1,4} - 2v_{1,3} + v_{1,2})/dx^2 &= 0 \\
 \tau v'_{1,4} + v_{1,4} - \lambda_1^2(v_{3,1} - 2v_{1,4} + v_{1,3})/dx^2 &= 0 \\
 \tau v'_{2,1} + v_{2,1} - \lambda_2^2(v_{2,2} - v_{2,1})/dx^2 &= 0 \\
 \tau v'_{2,2} + v_{2,2} - \lambda_2^2(v_{2,3} - 2v_{2,2} + v_{2,1})/dx^2 &= 0 \\
 \tau v'_{2,3} + v_{2,3} - \lambda_2^2(v_{2,4} - 2v_{2,3} + v_{2,2})/dx^2 &= 0 \\
 \tau v'_{2,4} + v_{2,4} - \lambda_2^2(v_{3,1} - 2v_{2,4} - v_{2,3})/dx^2 &= 0 \\
 \tau v'_{3,1} + v_{3,1} + \frac{a_2\lambda_2^2(v_{3,1} - v_{2,4}) - a_3\lambda_3^2(v_{3,2} - v_{3,1}) + a_1\lambda_1^2(v_{3,1} - v_{1,4})}{a_3dx^2} &= 0 \\
 \tau v'_{3,2} + v_{3,2} - \lambda_2^2(v_{3,3} - 2v_{3,2} + v_{3,1})/dx^2 &= 0 \\
 \tau v'_{3,3} + v_{3,3} - \lambda_3^2(v_{3,4} - 2v_{3,3} + v_{3,2})/dx^2 &= 0 \\
 \tau v'_{3,4} + v_{3,4} - (A_3/A_s)\lambda_3^2(v_{3,3} - v_{3,4})/dx^2 - I_{stim}/(gClA_s) &= 0
 \end{aligned} \tag{8.2}$$

where  $A_3 = 2\pi a_3 dx$ . We write this collection of equations as the linear system

$$\mathbf{v}'(t) = \mathbf{B}\mathbf{v}(t) + \mathbf{f}(t), \quad \mathbf{B} = (\mathbf{H} - \mathbf{I})/\tau, \quad \mathbf{f}(t) = I_{stim}(t)\mathbf{e}_{12}/(C_m A_s) \tag{8.3}$$

and  $\mathbf{H}$  is the Hines matrix

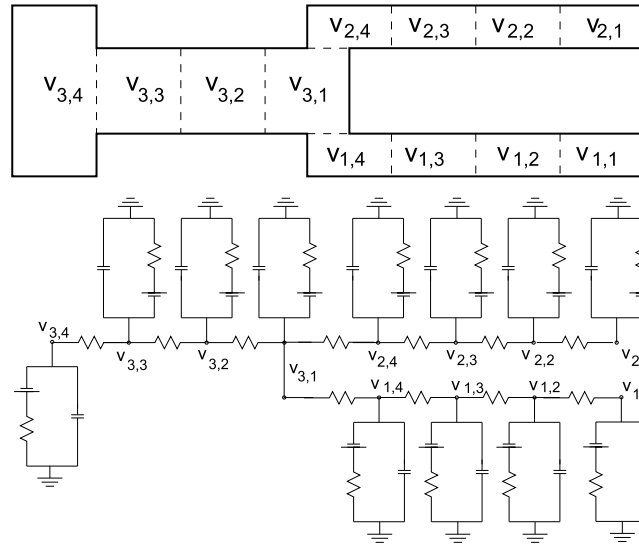


FIGURE 8.2 The compartmentalization of a branched cell with soma, and its associated circuit diagram.

$$\mathbf{H} = \frac{1}{dx^2} \begin{pmatrix} -\lambda_1^2 & \lambda_1^2 & 0 & 0 & 0 & 0 & 0 & 0 & 0 & 0 & 0 & 0 & 0 \\ \lambda_1^2 & -2\lambda_1^2 & \lambda_1^2 & 0 & 0 & 0 & 0 & 0 & 0 & 0 & 0 & 0 & 0 \\ 0 & \lambda_1^2 & -2\lambda_1^2 & \lambda_1^2 & 0 & 0 & 0 & 0 & 0 & 0 & 0 & 0 & 0 \\ 0 & 0 & \lambda_1^2 & -2\lambda_1^2 & 0 & 0 & 0 & 0 & \lambda_1^2 & 0 & 0 & 0 & 0 \\ 0 & 0 & 0 & 0 & -\lambda_2^2 & \lambda_2^2 & 0 & 0 & 0 & 0 & 0 & 0 & 0 \\ 0 & 0 & 0 & 0 & \lambda_2^2 & -2\lambda_2^2 & \lambda_2^2 & 0 & 0 & 0 & 0 & 0 & 0 \\ 0 & 0 & 0 & 0 & 0 & \lambda_2^2 & -2\lambda_2^2 & \lambda_2^2 & 0 & 0 & 0 & 0 & 0 \\ 0 & 0 & 0 & 0 & 0 & 0 & \lambda_2^2 & -2\lambda_2^2 & \lambda_2^2 & 0 & 0 & 0 & 0 \\ 0 & 0 & 0 & r_1\lambda_1^2 & 0 & 0 & 0 & r_2\lambda_2^2 & -c & \lambda_3^2 & 0 & 0 & 0 \\ 0 & 0 & 0 & 0 & 0 & 0 & 0 & 0 & \lambda_3^2 & -2\lambda_3^2 & \lambda_3^2 & 0 & 0 \\ 0 & 0 & 0 & 0 & 0 & 0 & 0 & 0 & 0 & \lambda_3^2 & -2\lambda_3^2 & \lambda_3^2 & 0 \\ 0 & 0 & 0 & 0 & 0 & 0 & 0 & 0 & 0 & 0 & \rho\lambda_3^2 & -\rho\lambda_3^2 & 0 \end{pmatrix}$$

where

$$r_1 = a_1/a_3 \quad r_2 = a_2/a_3 \quad c = r_1\lambda_1^2 + r_2\lambda_2^2 + \lambda_3^2 \quad \text{and} \quad \rho = A_3/A_s.$$

The genius of  $\mathbf{H}$  is at least double – it factors easily and is similar to a symmetric matrix. Regarding the former, we note that, as in the tridiagonal  $\mathbf{S}$  of Chapter 6, Gaussian Elimination applied to this matrix requires only one elimination per column.

## 8.2 EIGENVECTOR EXPANSION

We now describe the solution of Eq. (8.3) in terms of a series expansion in the eigenvectors of  $\mathbf{B}$ . Our expansion in the single fiber case made great use of the symmetry of  $\mathbf{S}$  and the resulting orthonormality of its eigenvectors. We recognize that although the soma and the branch point have rendered  $\mathbf{H}$  asymmetric it is nonetheless **similar** to a symmetric matrix. Let us unpack that last remark in the slightly more general context in which fiber  $j$  has  $N_j$  compartments and the soma represents an additional compartment attached to the mother. We note that

$$dx = \ell_j/N_j \quad \text{and} \quad N \equiv N_1 + N_2 + N_3 + 1,$$

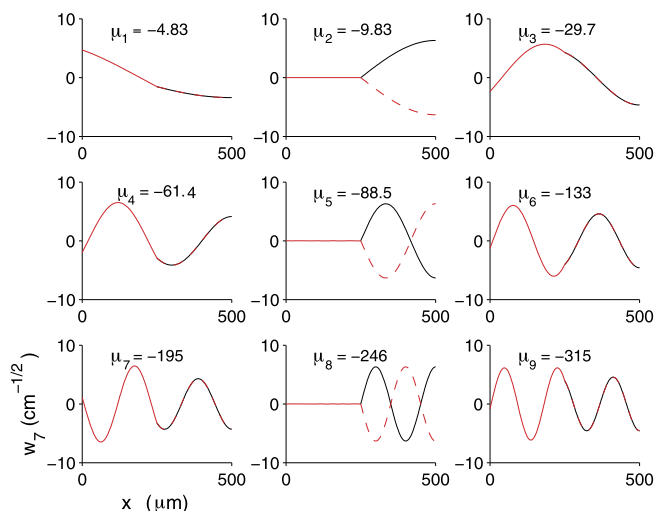


**FIGURE 8.3** The first nine (non-constant) eigenvectors,  $\mathbf{w}_n$ , and associated eigenvalues,  $\mu_n$ , of the Hines matrix  $\mathbf{H}$  for the cell described by Eqs. (8.7)–(8.8) and  $dx = 1 \mu\text{m}$ . Here the mother, branch 3, is depicted in red over the initial  $250 \mu\text{m}$  segment and the daughters, branch 1 in black and branch 2 in dashed red, are plotted over the second  $250 \mu\text{m}$ . These eigenvectors appear in two varieties. Either the two daughters are equal and opposite and the mother silent, or the daughters coincide and the mother plays along (in which case her slope at the soma is nonzero). (bevec.m)

define the diagonal matrix

$$\mathbf{D} = \text{diag}([a_1 \text{ones}(N_1, 1) \ a_2 \text{ones}(N_2, 1) \ a_3 \text{ones}(N_3, 1) \ a_3/\rho])$$

and note that  $\mathbf{DH} = (\mathbf{DH})^T = \mathbf{H}^T \mathbf{D}$ . This implies (Exercise 1) that

$$\mathbf{A} \equiv \mathbf{D}^{1/2} \mathbf{H} \mathbf{D}^{-1/2} \quad (8.4)$$

is symmetric. It follows, (Exercise 2), that if  $\{\mu_n, \mathbf{q}_n\}_{n=1}^N$  is the sequence of eigenpairs of  $\mathbf{A}$ , i.e.,  $\mathbf{A}\mathbf{q}_n = \mu_n \mathbf{q}_n$  then

$$\mathbf{H}\mathbf{w}_n = \mu_n \mathbf{w}_n \quad \text{where} \quad \mathbf{w}_n = \mathbf{D}^{-1/2} \mathbf{q}_n \quad (8.5)$$

and so the eigenvectors of  $\mathbf{H}$  are orthonormal in the weighted sense,

$$\mathbf{w}_n^T \mathbf{D} \mathbf{w}_m = \delta_{mn}. \quad (8.6)$$

We illustrate, in Figure 8.3, the first nine non-constant eigenvectors for the symmetric fork with

$$a_1 = a_2 = a_3 = 1 \mu\text{m}, \quad \ell_1 = \ell_2 = \ell_3 = 250 \mu\text{m} \quad \text{and} \quad A_s = 400\pi \mu\text{m}^2 \quad (8.7)$$

and passive cable parameters

$$C_m = 1 \mu\text{F}/\text{cm}^2, \quad g_{Cl} = 1/15 \text{ mS}/\text{cm}^2 \quad \text{and} \quad R_a = 0.3 \text{ k}\Omega \text{ cm}. \quad (8.8)$$

Regarding the representation of  $\mathbf{f}$  in terms of  $\mathbf{w}$ , we write

$$\mathbf{f}(t) = \sum_{n=0}^{N-1} \mathbf{c}_n(t) \mathbf{w}_n = \mathbf{D}^{-1/2} \sum_{n=0}^{N-1} \mathbf{c}_n(t) \mathbf{q}_n$$

and so find that  $\mathbf{c} = \mathbf{W}^T \mathbf{D} \mathbf{f}$ . Hence, with  $z_n = (\mu_n - 1)/\tau$ , and  $\mathbf{f}(t) = I_{stim}(t) \mathbf{e}_N / (C_m A_s)$ , it follows from Eq. (5.21) that

$$\mathbf{v}(t) = \frac{1}{2\pi dx C_m} \sum_{n=0}^{N-1} \mathbf{w}_n w_{n,N} \int_0^t I_{stim}(s) \exp((t-s)z_n) ds \quad (8.9)$$

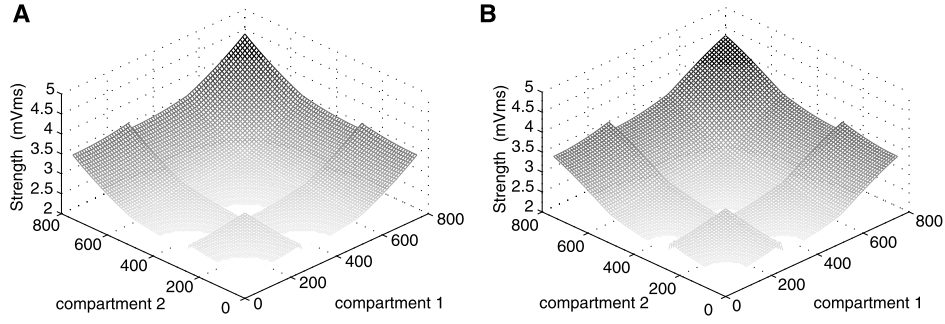


**FIGURE 8.4** The strength as a function of input location for the cell described by Eqs. (8.7)–(8.8). Compartments 1 to 250 correspond to daughter 1, 251 to 500 to daughter 2, and 501 to 750+1 to the mother and soma. We see that the strongest interactions occur for proximal (close to soma) inputs. For a fixed choice of  $c_1$  the strength increases as  $c_2$  approaches the soma. **A.** The full strength, Eq. (8.11). **B.** The strength computed by retaining only the  $n = 0$  and  $n = 1$  terms. We see that the leading order strength indeed captures all of the important detail of the full strength, and hence the first non-constant eigenvector,  $\mathbf{w}_1$ , is seen as the arbiter of synaptic integration. (bevec.m)

is the solution of the discrete passive dendrite equation, Eq. (8.3), with current injection at the soma. If we instead inject  $I_m(t)$  at compartment  $c_m$ , where  $m = 1, \dots, M$ , then the above takes the form

$$\mathbf{v}(t) = \frac{1}{2\pi dx C_m} \sum_{n=0}^{N-1} \mathbf{w}_n \sum_{m=1}^M w_{n,c_m} \int_0^t I_m(s) \exp((t-s)z_n) ds.$$

With this we investigate the interaction of pairs of simple inputs. In particular if we place the pair of equal impulses

$$I_1(t) = I_2(t) = \gamma \delta(t - t_1)$$

at compartments  $c_1$  and  $c_2$  then

$$\mathbf{v}(t) = \frac{\gamma \mathbb{1}_{(t_1, \infty)}(t)}{2\pi dx C_m} \sum_{n=0}^{N-1} \mathbf{w}_n (w_{n,c_1} + w_{n,c_2}) \exp((t - t_1)z_n). \quad (8.10)$$

We quantify their interaction by considering the strength of the soma response

$$S(c_1, c_2) \equiv \int_0^\infty v_N(t) dt = \frac{-\gamma}{2\pi dx C_m} \sum_{n=0}^{N-1} \frac{w_{n,N}}{z_n} (w_{n,c_1} + w_{n,c_2}). \quad (8.11)$$

We see that the strength at the soma, associated with simultaneous impulsive current injections, is a weighted average of the individual eigeninteractions,  $w_{n,N}(w_{n,c_1} + w_{n,c_2})$ , of the input,  $c_1$  and  $c_2$  and output,  $N$ , elements. We can “see” these terms, for small  $n$ , in the eigenvectors plotted in Figure 8.3. Note that the  $N$ th component, corresponding to the soma, appears at the far left in each plot. As  $w_{2,N} = w_{5,N} = w_{8,N} = 0$  and the other  $w_{n,N}$  are small compared to  $w_{1,N}$  we may be able to capture the salient interactions by retaining only the  $\mathbf{w}_0$  and  $\mathbf{w}_1$  terms in Eq. (8.11). This surmise is further supported by the fact that the interactions are scaled by  $z_n = (\mu_n - 1)/\tau$  where the  $\mu_n$  are eigenvalues, see Figure 8.3, increase rapidly in magnitude. It follows that  $w_{1,N}/z_1$  is more than 20 times its next term,  $w_{3,N}/z_3$ . We exploit these observations in Figure 8.4 where we contrast the full strength, Eq. (8.11), with the leading order strength associated with retaining the  $n = 0$  and  $n = 1$  terms.

## 8.3 NUMERICAL METHODS

We may solve Eq. (8.3) via the trapezoid rule, precisely as in Eq. (6.24). As an application we investigate the integration of 10 current pulses at distinct times and places. More precisely, we suppose that our right hand side

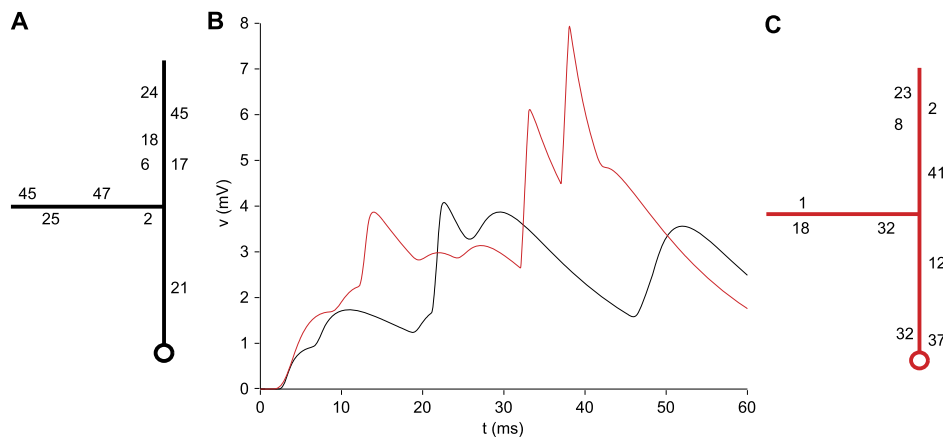


**FIGURE 8.5** The somatic response, in **B**, of the cell described by Eqs. (8.7)–(8.8) to current injection of the form Eq. (8.12) of amplitude  $I_0 = 100$  pA at the sites and times indicated in **A** and **C**. We observe smooth integration of distal early inputs punctuated by sharp increases immediately following proximal input. (trapfork.m)

takes the form

$$\mathbf{f}(t) = \frac{I_0}{2\pi a_1 dx C_m} \sum_{k=1}^{10} \mathbf{e}_{c_k} \mathbb{1}_{(t_k, t_{k+1})}(t) \quad (8.12)$$

where  $c_k$  denotes the compartment number of the  $k$ th stimulus,  $\mathbf{e}_{c_k}$  is defined as in Eq. (6.10), and compute, see Figure 8.5, the response at the cell body.

If rather than multi-site current injection we suppose polysynaptic input then we must solve

$$\mathbf{v}'(t) + \sum_{k=1}^K c_{syn,k}(t)(\mathbf{v}(t) - v_{syn})\mathbf{e}_{c_k} = \mathbf{B}\mathbf{v}(t) \quad (8.13)$$

where, with  $a_{b_k}$  denoting the radius of the branch that receives the  $k$ th input,

$$c_{syn,k}(t) = \frac{g_{syn,k}(t)}{2\pi a_{b_k} dx C_m}.$$

We solve this via the trapezoid rule precisely as we did in §6.5. In particular, we implement Eq. (6.56) where, now,  $\mathbf{B} = (\mathbf{H} - \mathbf{I})/\tau$ , and  $g_{syn,k}(t)$  is an alpha function

$$g_{syn,k}(t, t_k) = \bar{g}_{syn}((t - t_k)/\tau_\alpha) \exp(1 - (t - t_k)/\tau_\alpha) \mathbb{1}_{(t_k, \infty)}(t)$$

that commences from  $t_k$ . We illustrate our findings in Figure 8.6.

We observe, in Figure 8.6, that the early stimulus into branch 1 indeed depolarizes branch 2 and that the combined response attenuates as it approaches the soma. We investigate, in Figure 8.7, the difference between peak synaptic and peak somatic potentials as the synapse moves away from the soma.

## 8.4 THE PASSIVE DENDRITE EQUATION

As we pass to the limit of infinitely many infinitely short compartments we arrive (precisely as in §6.4) at 3 cable equations

$$\tau \frac{\partial v_j}{\partial t}(x, t) + v_j(x, t) = \lambda_j^2 \frac{\partial^2 v_j}{\partial x^2}(x, t), \quad 0 < x < \ell_j, \quad j = 1, 2, 3,$$

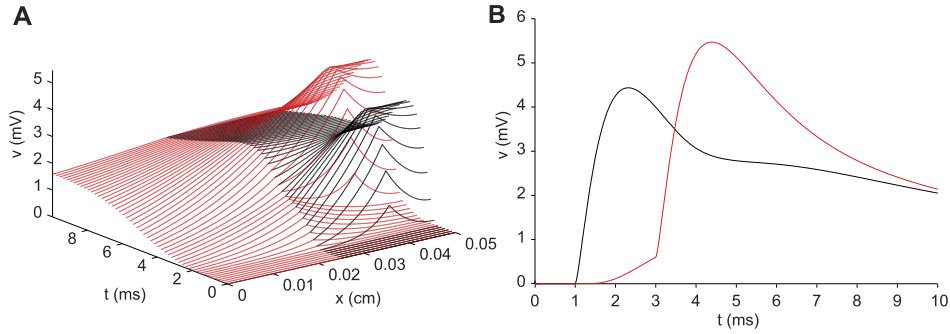


**FIGURE 8.6** The response of the cell described by Eqs. (8.7)–(8.8) to alpha synaptic input onto the two daughter branches, with  $\bar{g}_{syn} = 1$  nS,  $\tau_\alpha = 0.5$  ms,  $t_1 = 1$  and  $t_2 = 3$  ms and reversal potential  $v_{syn,k} = 70$  mV. Both inputs are located  $100 \mu\text{m}$  from the branch ends. **A.** Full space–time response. The response of the mother (branch 3) is plotted in red over the first  $250 \mu\text{m}$ . The response of the two daughters is plotted over the second  $250 \mu\text{m}$  with the response of branch 1 in black and that of branch 2 in red. **B.** The response in time at the two sites of stimulation, with black and red denoting branches 1 and 2 respectively, as in **A.** (trapforksyn.m)

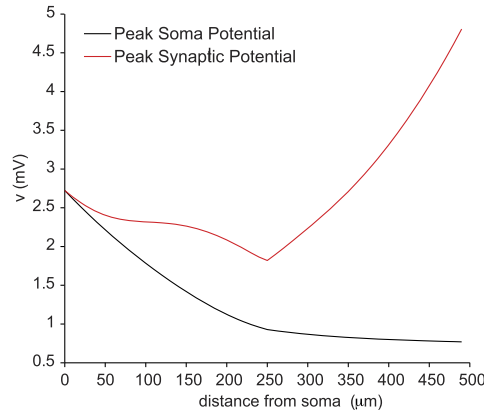


**FIGURE 8.7** Peak somatic and synaptic potentials for the cell described by Eqs. (8.7)–(8.8), as a function of the distance from the soma to the site of a single alpha synapse, with  $\bar{g}_{syn} = 0.5$  nS and  $\tau_\alpha = t_1 = 1$  ms. The steep decrease in peak soma potential as the synapse travels away from the soma diminishes as the synapse enters a daughter branch and the peak synaptic potential grows as the synapse approaches the sealed end. We have seen such “end effects” before in Figure 6.3A. (trapforksyngain.m)

for the three space–time potential functions,  $v_1$ ,  $v_2$  and  $v_3$ . The two daughters are sealed at their distal ends, i.e.,

$$\frac{\partial v_1}{\partial x}(0, t) = \frac{\partial v_2}{\partial x}(0, t) = 0.$$

The mother’s proximal end reflects the soma condition

$$\tau \frac{\partial v_3}{\partial t}(\ell_3, t) + v_3(\ell_3, t) + a_3 \lambda_3^2 (2\pi/A_s) \frac{\partial v_3}{\partial x}(\ell_3, t) = I_{stim}(t)/(gClA_s).$$

At the junction where the three branches meet we enforce current balance

$$a_1 \lambda_1^2 \frac{\partial v_1}{\partial x}(\ell_1, t) + a_2 \lambda_2^2 \frac{\partial v_2}{\partial x}(\ell_2, t) = a_3 \lambda_3^2 \frac{\partial v_3}{\partial x}(0, t),$$

and continuity of potential

$$v_1(\ell_1, t) = v_2(\ell_2, t) = v_3(0, t).$$

It can be advantageous to work in the non-dimensional variables

$$X \equiv x/\lambda_j, \quad L_j \equiv \ell_j/\lambda_j, \quad T \equiv t/\tau, \quad h \equiv a_3 \lambda_3^2 (2\pi/A_s). \quad (8.14)$$

For then the associated response and stimulus,

$$u_j(X, T) \equiv v_j(x, t), \quad J(T) \equiv I_{stim}(t)$$

obey

$$\frac{\partial u_j}{\partial T}(X, T) + u_j(X, T) = \frac{\partial^2 u_j}{\partial X^2}(X, T), \quad 0 < X < L_j \quad (8.15)$$

subject to the two sealed end conditions

$$\frac{\partial u_1}{\partial X}(0, T) = \frac{\partial u_2}{\partial X}(0, T) = 0, \quad (8.16)$$

the soma condition

$$\frac{\partial u_3}{\partial T}(L_3, T) + u_3(L_3, T) + h \frac{\partial u_3}{\partial X}(L_3, T) = J(T)/(g_{Cl}A_s), \quad (8.17)$$

and the junction conditions

$$\begin{aligned} a_1^{3/2} \frac{\partial u_1}{\partial X}(L_1, T) + a_2^{3/2} \frac{\partial u_2}{\partial X}(L_2, T) &= a_3^{3/2} \frac{\partial u_3}{\partial X}(0, T) \\ u_1(L_1, T) &= u_2(L_2, T) = u_3(0, T). \end{aligned} \quad (8.18)$$

Before proceeding to solve this general problem we pause to consider an important special case.

## 8.5 THE EQUIVALENT CYLINDER\*

We observe that the fork can be collapsed to a single cable, or cylinder, under a pair of simple geometric assumptions. We assume, for ease of presentation, that the only stimulus is current into the soma.

(EC1) If the two daughters have equal electrotonic lengths, i.e.,  $L_1 = L_2$ , we may define

$$U(X, T) = \begin{cases} \frac{a_1^{3/2} u_1(X, T) + a_2^{3/2} u_2(X, T)}{a_1^{3/2} + a_2^{3/2}}, & 0 < X < L_1 \\ u_3(X - L_1, T), & L_1 < X < L_1 + L_3 \end{cases} \quad (8.19)$$

and note that it obeys, with  $L \equiv L_1 + L_3$ ,

$$\begin{aligned} \frac{\partial U}{\partial T}(X, T) + U(X, T) &= \frac{\partial^2 U}{\partial X^2}(X, T), \quad 0 < X < L_1, \quad L_1 < X < L \\ U(L_1^-, T) &= U(L_1^+, T) \\ (a_1^{3/2} + a_2^{3/2}) \frac{\partial U}{\partial X}(L_1^-, T) &= a_3^{3/2} \frac{\partial U}{\partial X}(L_1^+, T) \\ \frac{\partial U}{\partial X}(0, T) &= 0, \quad \frac{\partial U}{\partial T}(L, T) + U(L, T) + h \frac{\partial U}{\partial X}(L, T) = J(T)/(g_{Cl}A_s). \end{aligned}$$

The third condition predicts a break in the slope of  $U$  if  $a_1^{3/2} + a_2^{3/2} \neq a_3^{3/2}$ .

(EC2) If the cell obeys the “3/2 law,” i.e.,  $a_1^{3/2} + a_2^{3/2} = a_3^{3/2}$  then  $U$  is simply the solution to

$$\begin{aligned} \frac{\partial U}{\partial T}(X, T) + U(X, T) &= \frac{\partial^2 U}{\partial X^2}(X, T), \quad 0 < X < L, \quad 0 < T \\ \frac{\partial U}{\partial X}(0, T) &= 0, \quad 0 < T \\ \frac{\partial U}{\partial T}(L, T) + U(L, T) + h \frac{\partial U}{\partial X}(L, T) &= J(T)/(g_{Cl}A_s), \quad 0 < T \\ U(X, 0) &= 0, \quad 0 < X < L. \end{aligned} \quad (8.20)$$

This system, Eq. (8.20), is known as the **Equivalent Cylinder Problem**. We solve it, as in §6.4, by proceeding from the hope that  $U(X, T) = q(X)p(T)$ . This hope necessitates

$$\begin{aligned} p'(T)/p(T) + 1 &= q''(X)/q(X), \quad 0 < X < L \\ q'(0) = 0, \quad p'(T)/p(T) + 1 + hq'(L)/q(L) &= J(T)/(g_{Cl}A_s p(T)q(0)) \end{aligned}$$

If, as in §6.4, we label by  $\vartheta$  the common value of  $q''(X)/q(X)$  and  $p'(T)/p(T) + 1$  then we see that it too must appear in the boundary condition for  $q$ . That is, we are compelled to consider

$$q''(X) = \vartheta q(X), \quad q'(0) = 0, \quad hq'(L) + \vartheta q(L) = 0. \quad (8.21)$$

This produces only a minor inconvenience, for the eigenfunction must still be of the form

$$q_n(X) = b_n \cos(\sqrt{-\vartheta_n} X) \quad (8.22)$$

and  $\vartheta_n$  is chosen to guarantee  $hq'_n(L) = -\vartheta_n q_n(L)$ . More precisely,  $\vartheta_n$  is the negative of the square of each root of

$$F(z) \equiv z + h \tan(zL). \quad (8.23)$$

We shall demonstrate (in Exercise 5) that these roots are simple and deduce (in Exercise 6) that

$$(\vartheta_m - \vartheta_n) \left( q_m(L)q_n(L)/h + \int_0^L q_m(X)q_n(X) dX \right) = 0, \quad (8.24)$$

and hence that the eigenfunctions are orthogonal with respect to the inner product

$$\langle f, g \rangle \equiv f(L)g(L)/h + \int_0^L f(X)g(X) dX. \quad (8.25)$$

We next normalize these eigenfunctions by choosing the  $b_n$  in Eq. (8.22) such that  $\langle q_n, q_n \rangle = 1$ , that is, such that

$$b_n^2 \left( \cos^2(\sqrt{-\vartheta_n} L)/h + \int_0^L \cos^2(\sqrt{-\vartheta_n} X) dX \right) = 1. \quad (8.26)$$

As with the straight cable, the naive guess that  $U(X, T) = q(X)p(T)$  has led us to the better guess

$$U(X, T) = \sum_{m=0}^{\infty} p_m(T)q_m(X). \quad (8.27)$$

On taking the inner product, Eq. (8.25), of each side with  $q_n$  we deduce from  $\langle q_m, q_n \rangle = \delta_{mn}$  that

$$\langle U, q_n \rangle = U(L, T)q_n(L)/h + \int_0^L U(X, T)q_n(X) dX = p_n(T)\langle q_n, q_n \rangle = p_n(T). \quad (8.28)$$

We now differentiate this with respect to time,  $T$ , and use Eq. (8.20) to replace time derivatives of  $U$  with space derivatives of  $U$ , and arrive at

$$\begin{aligned} p_n'(T) &= \frac{\partial U}{\partial T}(L, T)q_n(L)/h + \int_0^L \frac{\partial U}{\partial T}(X, T)q_n(X) dX \\ &= \left\{ J(T)/(g_{Cl}A_s) - U(L, T) - h \frac{\partial U}{\partial X}(L, T) \right\} q_n(L)/h + \int_0^L \left\{ \frac{\partial^2 U}{\partial X^2}(X, T) - U(X, T) \right\} q_n(X) dX \\ &= \left\{ J(T)/(g_{Cl}A_s) - h \frac{\partial U}{\partial X}(L, T) \right\} q_n(L)/h - p_n(T) + \int_0^L \frac{\partial^2 U}{\partial X^2}(X, T)q_n(X) dX. \end{aligned}$$

To this we apply integration by parts, in Exercise 7, to shift derivatives from  $U$  onto  $q_n$  and so find

$$\int_0^L \frac{\partial^2 U}{\partial X^2}(X, T)q_n(X) dX = \frac{\partial U}{\partial X}(L, T)q_n(L) + \vartheta_n p_n(T). \quad (8.29)$$

It then follows that  $p_n$  obeys the familiar, Eq. (2.13), ordinary differential equation

$$p_n'(T) + (1 - \vartheta_n)p_n(T) = J(T)q_n(L)/(g_{Cl}A_s h). \quad (8.30)$$

Its solution, per Eq. (3.2), is the simple convolution,

$$p_n(T) = \frac{q_n(L)}{g_{Cl}A_s h} \int_0^T J(s) \exp((T-s)(\vartheta_n - 1)) ds.$$

On inserting this into Eq. (8.27) we find that

$$U(X, T) = \sum_{n=0}^{\infty} \frac{q_n(L)q_n(X)}{g_{Cl}A_s h} \int_0^T J(s) \exp((T-s)(\vartheta_n - 1)) ds \quad (8.31)$$

solves the equivalent cylinder with soma problem, Eq. (8.20).

## 8.6 BRANCHED EIGENFUNCTIONS\*

We return to the full non-dimensional system of §8.4 and pose and solve the eigenproblem for

$$\mathbf{q}(X) = (q_1(X) \ q_2(X) \ q_3(X))^T.$$

Each component obeys the elemental branch condition

$$q_j''(X) = \vartheta q_j(X), \quad 0 < X < L_j \quad (8.32)$$

subject to the joint and seal conditions

$$\begin{aligned} q_1'(0) = q_2'(0) = h q_3'(L_3) + \vartheta q_3(L_3) &= 0 \\ q_1(L_1) = q_2(L_2) = q_3(0) & \\ a_1^{3/2} q_1'(L_1) + a_2^{3/2} q_2'(L_2) = a_3^{3/2} q_3'(0). & \end{aligned} \quad (8.33)$$

Just as eigenvectors of the Hines matrix were orthogonal in the weighted sense, Eq. (8.6), we find (Exercise 10) that  $\mathbf{q}_m$  is orthogonal to  $\mathbf{q}_n$  in the weighted inner product

$$\langle (f_1 \ f_2 \ f_3), (g_1 \ g_2 \ g_3) \rangle \equiv a_3^{3/2} f_3(L_3)g_3(L_3)/h + \sum_{j=1}^3 a_j^{3/2} \int_0^{L_j} f_j(X)g_j(X) dX. \quad (8.34)$$

Arguing in precisely the same fashion as the previous section, we find that the full solution of the passive dendrite, subject to somatic current injection, may be expressed as

$$u(X, T) = \sum_{n=0}^{\infty} \frac{\mathbf{q}_n(X) q_{n,3}(L_3)}{g_{Cl} A_s h} \int_0^T J(s) \exp((T-s)(\vartheta_n - 1)) ds. \quad (8.35)$$

This is the natural three-dimensional analog of the response, Eq. (8.31), of the equivalent cylinder. To help fix ideas we now compute these branched eigenfunctions for dendrites whose branches have equal electrotonic lengths, i.e.,  $L_1 = L_2 = L_3 = L$ .

**Without soma.** We begin, for simplicity, by removing the soma. As  $A_s \rightarrow 0$  we find  $h \rightarrow \infty$  and so  $q'_3(L) = 0$ . In this case,

$$q_1 = b_1 \cos(\sqrt{-\vartheta} X), \quad q_2 = b_2 \cos(\sqrt{-\vartheta} X), \quad \text{and} \quad q_3 = b_3 \cos(\sqrt{-\vartheta} (L - X))$$

and so continuity at the joint requires

$$b_1 \cos(\sqrt{-\vartheta} L) = b_2 \cos(\sqrt{-\vartheta} L) = b_3 \cos(\sqrt{-\vartheta} L) \quad (8.36)$$

while Kirchhoff's Current Law at the joint requires

$$-a_1^{3/2} \sqrt{-\vartheta} b_1 \sin(\sqrt{-\vartheta} L) - a_2^{3/2} \sqrt{-\vartheta} b_2 \sin(\sqrt{-\vartheta} L) = a_3^{3/2} \sqrt{-\vartheta} b_3 \sin(\sqrt{-\vartheta} L). \quad (8.37)$$

There now appears a natural splitting. In particular, if  $\cos(\sqrt{-\vartheta} L) = 0$  then (8.36) holds and the  $b_j$  are constrained by (8.37). This is one linear equation in three unknowns and so defines a plane. The upshot is that each eigenvalue has two linearly independent eigenfunctions. To be precise

$$\vartheta_n = -\frac{n^2 \pi^2}{4L^2}, \quad \mathbf{q}_n(X) = b_n^1 \mathbf{q}_n^1(X) + b_n^2 \mathbf{q}_n^2(X) \quad n = 1, 3, 5, \dots \quad (8.38)$$

where

$$\mathbf{q}_n^1(X) = \begin{pmatrix} \cos(\sqrt{-\vartheta_n} X) \\ 0 \\ -(a_1/a_3)^{3/2} \cos(\sqrt{-\vartheta_n} (L - X)) \end{pmatrix}$$

and

$$\mathbf{q}_n^2(X) = \begin{pmatrix} 0 \\ \cos(\sqrt{-\vartheta_n} X) \\ -(a_2/a_3)^{3/2} \cos(\sqrt{-\vartheta_n} (L - X)) \end{pmatrix}. \quad (8.39)$$

We note that the continuity equation is satisfied by the vanishing of each term in the second condition of Eq. (8.33). The analogous satisfaction of current balance at the joint requires  $\sin(\sqrt{-\vartheta} L) = 0$  in which case continuity requires  $b_1 = b_2 = b_3$  and we find

$$\vartheta_n = -\frac{n^2 \pi^2}{4L^2} \quad n = 2, 4, 6, \dots$$

$$\mathbf{q}_n(X) = b \begin{pmatrix} \cos(\sqrt{-\vartheta_n} X) \\ \cos(\sqrt{-\vartheta_n} X) \\ \cos(\sqrt{-\vartheta_n} (L - X)) \end{pmatrix}$$

where  $b$  is the arbitrary normalization constant. In summary, we note that the eigenvalues are  $-n^2 \pi^2 / (2L)^2$  for  $n = 0, 1, 2, \dots$  and that these are simple for even  $n$  and double for odd  $n$ .

**With soma.** If we now attach the soma we find that the eigenfunction of branch 3 must be of the form

$$q_3(X) = b_3 \{ \cos(\sqrt{-\vartheta} (L - X)) + (\sqrt{-\vartheta} / h) \sin(\sqrt{-\vartheta} (L - X)) \}.$$

It follows that continuity at the joint requires

$$b_1 \cos(\sqrt{-\vartheta} L) = b_2 \cos(\sqrt{-\vartheta} L) = b_3 \{ \cos(\sqrt{-\vartheta} L) + (\sqrt{-\vartheta}/h) \sin(\sqrt{-\vartheta} L) \} \quad (8.40)$$

while Kirchhoff's Current Law there requires

$$-a_1^{3/2} b_1 \sin(\sqrt{-\vartheta} L) - a_2^{3/2} b_2 \sin(\sqrt{-\vartheta} L) = a_3^{3/2} b_3 \{ \sin(\sqrt{-\vartheta} L) - (\sqrt{-\vartheta}/h) \cos(\sqrt{-\vartheta} L) \}. \quad (8.41)$$

As above, there is a natural splitting. If  $\cos(\sqrt{-\vartheta} L) = 0$  then (8.40) implies that  $b_3 = 0$  and (8.41) then requires that  $a_1^{3/2} b_1 + a_2^{3/2} b_2 = 0$  and so

$$\vartheta_n = -\frac{n^2 \pi^2}{4L^2} \quad n = 1, 3, 5, \dots$$

$$\mathbf{q}_n(X) = b \cos(\sqrt{-\vartheta_n} X) \begin{pmatrix} 1 \\ -(a_1/a_2)^{3/2} \\ 0 \end{pmatrix}.$$

We recognize these eigenfunctions in panels  $\mu_2$ ,  $\mu_5$  and  $\mu_8$  in Figure 8.3. The zero in  $\mathbf{q}_n$  (third component) has interesting consequences for branch to branch communication. In particular, any stimulus of the form

$$J(X, T) = \sum_{m=1}^{\infty} J_m(T) \mathbf{q}_{2m-1}(X), \quad (8.42)$$

with  $J_m(T)$  arbitrary, will be invisible to the mother and therefore the soma. See Exercise 9.

Next, if  $\cos(\sqrt{-\vartheta} L) \neq 0$  then (8.40) implies that

$$b_1 = b_2 = b_3 (1 + (\sqrt{-\vartheta}/h) \tan(\sqrt{-\vartheta} L))$$

and (8.41) that

$$-a_1^{3/2} b_1 \tan(\sqrt{-\vartheta} L) - a_2^{3/2} b_2 \tan(\sqrt{-\vartheta} L) = a_3^{3/2} b_3 (\tan(\sqrt{-\vartheta} L) - \sqrt{-\vartheta}/h).$$

Combining these two we find that  $\vartheta$  is the negative of the square of each root of

$$F(z) \equiv (1 + (z/h) \tan(zL)) \tan(zL) (a_1^{3/2} + a_2^{3/2}) + a_3^{3/2} (\tan(zL) - z/h),$$

the branched analog of Eq. (8.23). The associated eigenfunction is

$$\mathbf{q}_n(X) = b \begin{pmatrix} \cos(\sqrt{-\vartheta_n} X) \\ \cos(\sqrt{-\vartheta_n} X) \\ \frac{\cos(\sqrt{-\vartheta_n}(L-X))}{1 + (\sqrt{-\vartheta_n}/h) \tan(\sqrt{-\vartheta_n} L)} \end{pmatrix}$$

where  $b$  is the normalization constant. We recognize these eigenfunctions in panels  $\mu_1$ ,  $\mu_3$ ,  $\mu_4$ ,  $\mu_6$ ,  $\mu_7$  and  $\mu_9$  in Figure 8.3.

## 8.7 SUMMARY AND SOURCES

We have added a soma and a pair of branches to our passive cable and demonstrated that each of the analytical and computational approaches developed for the cable apply, with little change, to the passive dendrite with soma. The only real change is the replacement of the second difference matrix with the Hines matrix and the fact that the eigenvectors of the latter are considerably more complicated than those of the straight cable. We have restricted attention to the three branched fork solely for reasons of exposition. For each of the fundamental constructs makes

perfect sense in larger trees. In particular, [Hines \(1984\)](#), solves the compartmental ordering problem for general trees. Rall, see [Segev et al. \(1994\)](#), solves the Equivalent Cylinder problem for reducible trees and [von Below \(1988\)](#) establishes the inner product in which the branched eigenfunctions of general trees are orthogonal. Exercise 11 is drawn from [Nicaise \(1987\)](#).

## 8.8 EXERCISES

1. Regarding the lead up to Eq. (8.4), show that  $\mathbf{DH}$  is indeed symmetric and deduce the symmetry of  $\mathbf{A}$  from this. Do this by hand (without numbers) by drawing and exploiting the block structure of  $\mathbf{H}$ .
2. † Show that Eq. (8.5) and Eq. (8.6) indeed follow from Eq. (8.4).
3. † Integrate the response of the soma component to dual simultaneous current impulses and explain how Eq. (8.11) arises from Eq. (8.10).
4. † Although dendritic cable diameters and branching do not permit one to space-clamp the cell, it is not uncommon for experimentalists to employ voltage clamps at one or more sites. The most common site is the soma. With regard to our concrete compartmental system, Eq. (8.2), note that if we clamp the soma potential,  $v_{3,4}$ , to the value  $v_c$ , then the penultimate equation in (8.2) takes the form

$$\tau v'_{3,3} + v_{3,3} - \lambda_3^2(-2v_{3,3} + v_{3,2}) = \lambda_3^2 v_c / dx^2, \quad (8.43)$$

and that the final equation in (8.2) is no longer a constraint on the system (for  $v_{3,4}$  is already constrained) but is rather an expression for the current,  $I_c$ , that is necessary to hold  $v_{3,4}$  at  $v_c$ . In particular

$$I_c = g_{Cl} A_s v_c - g_{Cl} A_3 \lambda_3^2 (v_{3,3} - v_c) / dx^2. \quad (8.44)$$

The upshot of these 2 equations is that we now remove the last row and column of the Hines matrix,  $\mathbf{H}$ , and replace the stimulus vector,  $\mathbf{f}$  in Eq. (8.3) with

$$\mathbf{f}(t) = (\lambda_3 / dx)^2 v_c \mathbf{e}_{11} / \tau.$$

Please modify `trapforksyn.m` to permit a somatic voltage clamp and produce results like [Figure 8.8](#).

*Hint:* Note that the rest potential is nonzero and decreases away from the clamp. To find it, return to Eq. (8.3) and solve  $\mathbf{B}\mathbf{v}_r + \mathbf{f} = 0$ . This nonzero rest also has implications for the initialization of our trapezoid rule. Return to Eq. (6.23) to get it right.

5. The eigenvalues,  $\vartheta_n$ , of the equivalent cylinder with soma are determined by  $z_n$ , the roots of  $z/h + \tan(zL)$ , via  $\vartheta_n = -z_n^2$ . For representative  $L$  and  $h$  carefully graph the functions  $f(z) = \tan(zL)$  and  $g(z) = -z/h$  and argue that these two graphs intersect at infinitely many points,  $0 = z_0 < z_1 < z_2 < \dots$ . What number is  $z_n$  close to for large  $n$ ?
6. Establish the orthogonality, Eq. (8.24), of the eigenfunctions of the equivalent cylinder with soma by demonstrating that

$$\begin{aligned} \vartheta_n \int_0^L q_n(X) q_m(X) dX &= \int_0^L q_n''(X) q_m(X) dX \\ &= q_m(L) q_n(L) (\vartheta_m - \vartheta_n) / h + \vartheta_m \int_0^L q_n(X) q_m(X) dX. \end{aligned}$$

7. † Establish the validity of Eq. (8.29).
8. Consider a cell that satisfies the Equivalent Cylinder conditions. Rather than injecting current at the soma, we now inject equal current into the two daughters. In particular, we suppose

$$\frac{\partial u_j}{\partial T}(X, T) + u_j(X, T) - \frac{\partial^2 u_j}{\partial X^2}(X, T) = I_{stim}(X, T), \quad j = 1, 2$$

for some function  $I_{stim}$ . Derive a system of equations for the  $U$  of (8.19).

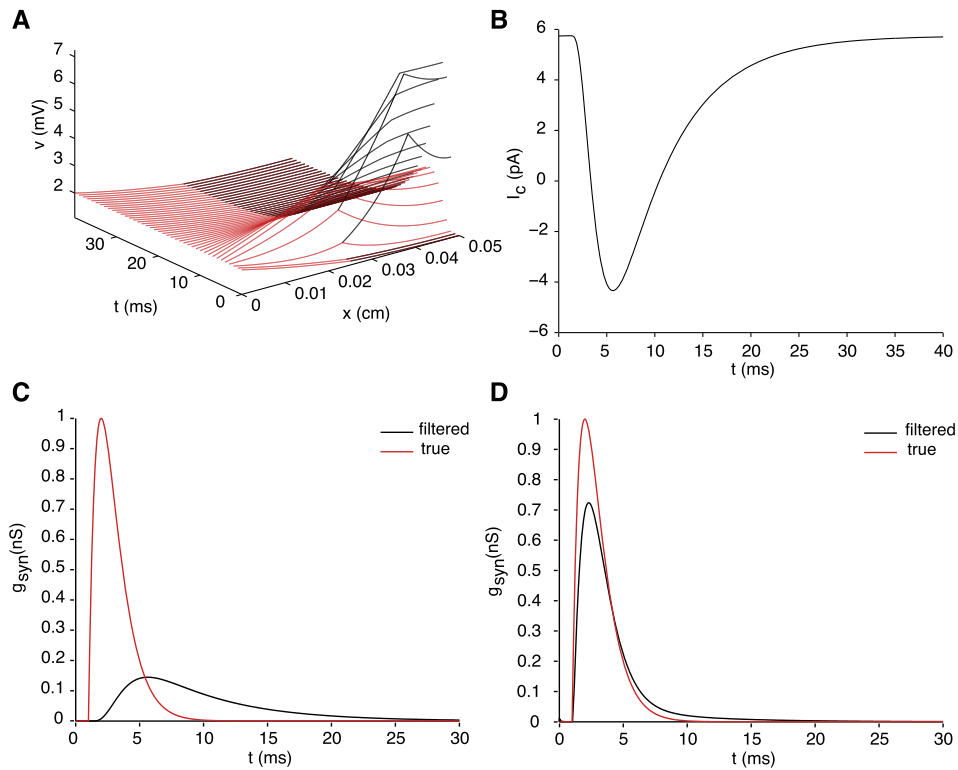


**FIGURE 8.8** A. Space-time illustration of the potential in the fork with the soma potential clamped at  $v_c = 2$  mV, and a distal ( $400 \mu\text{m}$ )  $\alpha$ -synapse with  $\bar{g}_{syn} = 1$  nS,  $\tau_\alpha = t_1 = 1$  ms and  $v_{syn} = 70$  mV. B. The associated clamp current at the soma, as computed by Eq. (8.44). This a beautiful signature of the distal excitatory input. On dividing it by the clamp potential we arrive, as in Chapter 4, at an estimate of the time varying conductance. In particular, in C and D we plot (in black) the “received” conductance  $g(t) = (I_c(t) - I_c(0))/(v_c - v_{syn})$ . C corresponds to the synapse of A while D is the same conductance but placed proximal ( $50 \mu\text{m}$ ). For comparison purposes we have included the true synaptic conductance, in red. The figures provide yet another window on the attenuation, or dendritic filtering, of synaptic inputs. (trapforksynclamp.m)

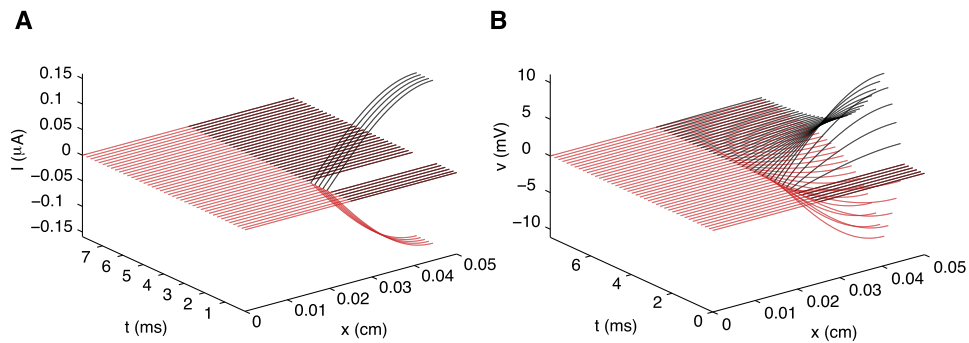


**FIGURE 8.9** An example of a stimulus (A) that does not reach the soma, see response in B. Color scheme as in Figure 8.8A. (trapforkd.m)

9. Modify `trapfork.m` to accept distributed current input. Assume equal electrotonic branch lengths and apply a stimulus of the form Eq. (8.42) and show that the mother is indeed kept in the dark.
10. † Establish the orthogonality of the branched eigenfunctions,  $\mathbf{q}_n$  obeying Eqs. (8.32)–(8.33), with regard to the inner product defined in Eq. (8.34).
11. It can be shown under fairly general hypotheses that the eigenvalues of a branched tree fall in two camps,  $\vartheta = -n^2\pi^2$  and  $\cos(\sqrt{-\vartheta}) = z_j$  where  $z_j$  is an eigenvalue, less than 1 in magnitude, of the **adjacency matrix**

associated with the tree. For our simple fork, the adjacency matrix is

$$\mathbf{A} = \frac{1}{\sqrt{a_1^{3/2} + a_2^{3/2} + a_3^{3/2}}} \begin{pmatrix} 0 & 0 & 0 & a_1^{3/4} \\ 0 & 0 & 0 & a_2^{3/4} \\ 0 & 0 & 0 & a_3^{3/4} \\ a_1^{3/4} & a_2^{3/4} & a_3^{3/4} & 0 \end{pmatrix}.$$

Confirm, using, e.g., the symbolic toolbox in MATLAB, that  $0, 0, 1, -1$  are the eigenvalues of  $\mathbf{A}$ . Reconcile this result with our findings in Eqs. (8.38)–(8.39).